Journal of Multifunctional Composites

Microstructure Image-Based Modeling of Fracture in Continuous Fiber-Reinforced Ceramic Matrix Composites

V. BHEEMREDDY[1], K. CHANDRASHEKHARA[1],[*] L. R. DHARANI[1] and G. E. HILMAS[2]

[1]*Department of Mechanical and Aerospace Engineering, Missouri University of Science and Technology, Rolla, MO 65409*
[2]*Department of Materials Science and Engineering, Missouri University of Science and Technology, Rolla, MO 65409*

KEYWORDS

continuous fiber-reinforced
  ceramic matrix composite
multi-scale modeling
microstructure image
object oriented finite element
  analysis
crack propagation
extended finite element method
cohesive damage modeling

ABSTRACT

The failure behavior of a continuous fiber-reinforced ceramic matrix composite (CFCC) is studied by the example of a unidirectionally reinforced SiC/SiC$_f$ composite. A multi-scale modeling framework is developed for evaluating damage at the micro-level. An actual fiber/matrix topology, based on a microstructure image, is used at the micro-level. A finite element mesh of the microstructure is generated using an object oriented finite element analysis tool. An extended finite element method, integrated with cohesive damage modeling, is used to study crack propagation in the microstructure. Finite element model validation using a benchmark study is discussed. The effect of matrix strength and matrix toughness on the stress-displacement behavior in the micromechanical model is studied. Cohesive parameters, cohesive strength, and fracture energy, of the micromechanical model are estimated from the constituent properties.

1. INTRODUCTION

The microstructure of a material controls its physical and mechanical properties [1]. Several analytical and numerical techniques have evolved to predict the behavior of multi-phase materials. Analytical models provide a reasonable estimate of material behavior, but are only applicable for simple phase configurations. Several micromechanical models have been developed over decades to predict the macromechanical behavior of a material. Often these methods are integrated with finite element simulations to extend the realm of problems that can be modeled, but these models rely on simplifying assumptions about the geometry/distribution/orientation of the microstructure. A novel approach, as an alternative to these traditional methods, is the use of image-based finite element analysis of microstructures wherein, a finite element mesh is generated directly on the microstructure of the material followed by subsequent analysis using the same microstructure mesh domain. An object oriented finite element analysis (OOF) tool has been developed at the Center for Theoretical and Computational Material Science, National Institute of Standards and Technology (NIST) to predict the material behavior and multiple other purposes using experimental/simulated microstructures [2–5]. OOF has been used to predict the thermal/mechanical behavior of a material by several investigators. Chawla *et al.* [1] have implemented OOF to predict the elastic constants of two materials—silicon carbide particle-reinforced aluminum matrix composites and double-cemented tungsten carbide particle-reinforced cobalt matrix composites. Levis and Geltmacher [6] have developed a three-dimensional spatial reconstruction of an austenitic steel microstructure and incorporated the image into OOF to study the mesomechanical response. Goel *et al.* [7] have used OOF to investigate the longitudinal elastic modulus of a glass fiber/polypropylene thermoplastic composite. The authors have compared the numerical results using the developed model with those of experimental results and results from other models. The authors have also concluded the significance of taking microstructural parameters into account for accurate prediction of longitudinal elastic modulus. Dong and Bhattacharyya [8] have implemented

*Corresponding author. E-mail: chandra@mst.edu, Phone: 573-341-4587

doi:10.12783/issn.2168-4286/2.4/Bheemreddy

1

OOF for predicting the tensile properties of polypropylene/ organoclay nanocomposites using the images from scanning electron microscopy (SEM) and transmission electron microscopy (TEM) studies. The authors have also compared their results with experimental results and theoretical composite models. Bakshi *et al.* [9] have estimated the overall elastic modulus of a spark plasma sintered tantalum carbide using a technique called scan-and-solve and compared their results with OOF.

The failure analysis of heterogeneous materials, accounting for damage initiation and evolution, has been explored by many researchers [10–16]. Advanced numerical methods have been developed to introduce an arbitrary discontinuity in the models for an effective analysis of material failure [16–27]. Cohesive damage models, based on traction-separation laws, were developed for simulating crack propagation through damage initiation and evolution. However, the major shortcoming of this approach is that it requires the potential crack path to be known *a priori*. Cohesive elements are inserted along these known paths, thereby limiting the application for evolving arbitrary discontinuities. Numerical methods on treating arbitrary cracks without any prior knowledge of crack paths were first developed by Belytschko *et al.* [15,18–20]. Crack tip enrichments were introduced for enhancing the nodal degrees of freedom, for effective description of element discontinuity displacement. This method is called as the extended finite element method (XFEM). This method is currently integrated into several commercial finite element software. Recently, Jung and Taciroglu [21] have developed a dynamic XFEM formulation for an arbitrary shaped inclusion. Other methods such as augmented finite element method (AFEM) and meshfree methods have also been integrated with cohesive zone elements to model the fracture behavior [22–27]. AFEM can model arbitrary discontinuities without requiring any enrichment functions. It preserves element locality and is promising to be integrated with commercial finite element software. Meshfree methods such as extended element-free Galerkin (XEFG) and extended meshfree methods have been developed to address arbitrary cracking phenomenon however these methods were computationally expensive.

In this study, a modeling framework based on XFEM and OOF was developed to study failure behavior in a CFCC

microstructure under a transverse tensile load. OOF was used to generate a finite element mesh of the microstructure. The uniqueness of this work is in integrating XFEM and OOF methods to simulate crack initiation and propagation in original microstructures. Michlik and Berndt [28] have proposed an integrated XFEM and OOF approach for thermal and structural analyses of microstructures in thermal barrier coatings. However, the authors have incorporated the XFEM formulation in an in-house code. In the current work, this approach is implemented in a commercial finite element tool—Abaqus v.6.12. Unlike conventionally used methods such as cohesive elements, the current approach does not require the crack path to be known *a priori*. The methods presented in this work have the potential to be extended to three dimensional microstructures. The paper is organized as follows. Finite element mesh generation of a microstructure is detailed in Section 2. Theoretical background on XFEM and the multi-scale framework are described in Section 3. Results are discussed in Section 4.

2. DOMAIN DISCRETIZATION OF MATERIAL MICROSTRUCTURE USING OOF

2.1 . OOF Framework for Domain Discretization

The domain discretization scheme used in OOF for generating the finite element mesh of a CFCC microstructure is shown in Figure 1. This procedure will enable clustering of various material phases or classifying grains from their boundaries, and thereby make the discretized image useful for further analysis using numerical simulations. The starting point in the discretization scheme is a gray-scale image. Each pixel of the image has a different gray level and the goal of domain discretization is to group pixels with similar intensities. Pixel selection is typically conducted by selecting an arbitrary pixel, and pixels with similar gray levels are highlighted for forming groups. In the 'microstructure' step the image is segmented by classifying the individual phases. After creating the microstructure, material properties can be assigned to each pixel or individual phases. The next step is to create a finite element mesh skeleton. In this step, the element type required (quadrilateral/triangular) and their positions can be specified. Using appropriate element
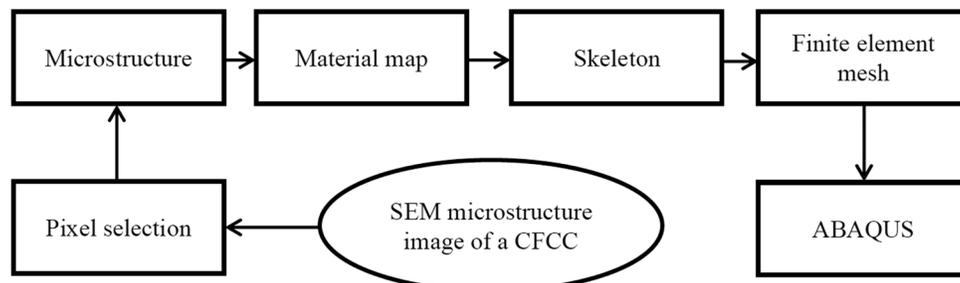

**Figure 1.** *Domain discretization scheme using OOF.*

refinement methods and node motion, a finite element mesh with good representation of associated geometry can be obtained. A skeleton is, however, not a complete finite element mesh and it contains no information about the finite element interpolation functions. Once a good mesh representation is obtained, an actual finite element mesh can be created from the skeleton. This step adds physics and math to the skeleton and a fully functional finite element mesh is created, which can be transferred to Abaqus v.6.12 for further study. The algorithms used for image segmentation are beyond the scope of this paper and are discussed elsewhere.

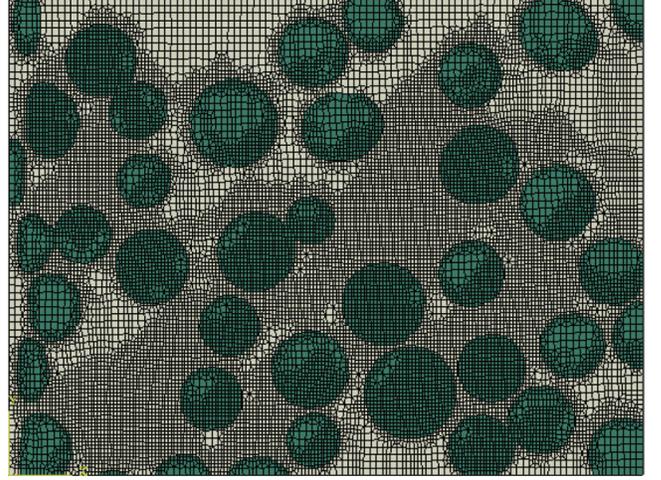## 2.2. Finite Element Mesh Generation of a CFCC Microstructure

OOF was used to generate finite element mesh of a microstructure image consisting of 1280 pixel × 1032 pixel. Figure 2 shows the SEM image of the transverse cross-section of a unidirectional CFCC microstructure.

The light and dark regions represent different material phases. The darker phase with circular regions corresponds to the fibers and the lighter phase is the matrix. These individual phases were clustered into separate pixel groups using the OOF framework. Pixel selection is conducted using 'circle' and 'ellipse' methods which allow grouping the pixels within the circular or elliptical domains. For the finite element mesh skeleton, a quadskeleton with 100 elements along the x-direction and 60 elements along the y-direction was developed as an initial mesh. The microstructure was coarse meshed with quadrilateral elements and mesh size was refined iteratively using various routines—refine, relax, snap nodes, and snap refine, to create a quality mesh conforming to material boundaries. Figure 3 shows the finite element mesh of the microstructure obtained using the above discretization scheme.

Two element functionals, shape energy and homogeneity
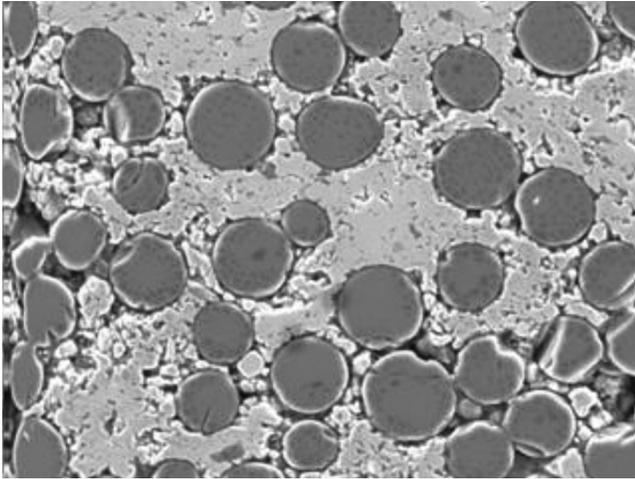
Figure 2. SEM microstructure image of a SiC fiber reinforced ZrB$_2$-ZrSi$_2$ matrix CFCC developed at Missouri S&T.

Figure 3. Finite element mesh of a CFCC microstructure.

energy, were used to quantify the quality of mesh generated. The former measures the quality of the shape of elements while the latter measures mesh compliance with boundaries. A mesh is considered to be of good quality if the summation of the weighted average of functionals is low. The shape energy functional (E_{shape}) favors low aspect ratio elements and was calculated for quadrilateral elements using [5],

$$E_{shape} = 1 - ((1 - w_{opp})q_{min} + w_{opp}q_{opp}) \quad (1)$$

$$q = 2\frac{A_1}{L_1^2 + L_2^2} \quad (2)$$

Where, q is the quality measured at each corner, q_{min} corresponds to a corner with minimum q, q_{opp} is the q measured at opposite corner, A_1 is the area of parallelogram formed by two edges adjacent to a corner, L_1 and L_2 are lengths of the adjacent sides to a corner, and $w_{opp} = 10^{-5}$ is an arbitrary parameter. The homogeneity functional (E_{hom}) was calculated using,

$$E_{hom} = 1 - H \quad (3)$$

$$H = \frac{max_i\{a_i\}}{A_2} \quad (4)$$

Here, a_i is the fraction of area of an element that conforms to material i, and A_2 is the area of element. The weighted sum of the two functionals gives effective element energy,

$$E = \alpha E_{hom} + (1 - \alpha)E_{shape} \quad (5)$$

Where, α is an adjustable parameter and 0.5 is the value used in this work [2].

3. XFEM BASED MULTI-SCALE MODELING FRAMEWORK

3.1. XFEM Method

The XFEM method is an effective numerical approach for discrete crack modeling problems, and is based on Galerkin and partition of unity concepts. This method involves local enrichment of approximation spaces, which becomes particularly useful for approximating solutions of computational domains with discontinuities and singularities. A discontinuity is defined here as a high gradient in a field quantity, in a local domain. In solids, these discontinuous field quantities are typically stresses/strains or displacements, due to interfaces or cracks. Using local enrichment, XFEM allows to model discontinuities in element interiors thereby not requiring to *a priori* define a mesh conforming to crack boundaries. Conventional finite element approaches often result in low convergence rates and exhibit poor accuracy in modeling these problems.

To understand how an enrichment function is added to the finite element approximation, a simple crack domain is considered as shown in Figure 4(a).

The objective is to represent the mesh in Figure 4(a) (Mesh A) using the mesh in Figure 4(b) (Mesh B). The finite element approximation for Mesh A is given by,

$$u^h = \sum_{i=1}^{10} N_i u_i \qquad (6)$$

Where, N_i and u_i are shape function and displacement vector, respectively, at node i. Two parameters, a_1 and a_2, are defined using,

$$a_1 = \frac{u_9 + u_{10}}{2} \quad \text{and} \quad a_2 = \frac{u_9 - u_{10}}{2} \qquad (7)$$

u_9 and u_{10} can be expressed in terms of a_1 and a_2 as,

$$u_9 = a_1 + a_2 \quad \text{and} \quad u_{10} = a_1 - a_2 \qquad (8)$$

The terms u_9 and u_{10} in Equation (8) are replaced in Equation (6) to get,

$$u^h = \sum_{i=1}^{8} N_i u_i + a_1 (N_9 + N_{10}) + a_2 (N_9 + N_{10}) H(x) \qquad (9)$$

Where, $H(x)$ is a discontinuous jump function defined as,

$$H(x) = \begin{cases} 1, & y > 0 \\ -1, & y < 0 \end{cases} \qquad (10)$$

Now, $a_1 = (u_9 + u_{10})/2$ in Mesh A can be replaced by u_{11} in Mesh B. Similarly, $N_9 + N_{10}$ can be replaced by N_{11}. Accordingly, the finite element approximation for Mesh B is given by,

$$u^h = \sum_{i=1}^{8} N_i u_i + N_{11} u_{11} + a_2 N_{11} H(x) \qquad (11)$$

The first two terms on the right-hand side of Equation (11) correspond to a standard finite element approximation and the third term is a discontinuous enrichment. This equation is equivalent to a standard finite element approximation for Mesh B with an additional discontinuous enrichment term. Similar to the discontinuity enrichment, XFEM approximation uses a crack tip enrichment term. Figure 5 shows the nodal enrichment representation (discontinuity and crack tip) in a crack domain.

Overall, the XFEM based enriched finite element approximation is generalized and is given by [29],

$$u = \sum_{i \in \Omega} N_i(x) \left[u_i + \underbrace{H(x) a_i}_{i \in \Omega_d} + \underbrace{\sum_{j=1}^{4} F_j(x) b_i^j}_{i \in \Omega_c} \right] \qquad (12)$$

Here, N_i is the shape function, u_i is the displacement vector, $H(x)$ is the jump function or discontinuity function, $F_j(x)$ is the crack tip enrichment function, a_i and b_i are nodal enriched degree of freedom vectors corresponding to discontinuous enrichment function and crack tip enrichment function respectively. The standard finite element approximation is applicable for all the nodes (Ω) in the model, crack tip enrichment function is applicable for set of all nodes (Ω_c) with shape function supports cut by crack tip, and discontinuity enrichment function is for set of all nodes (Ω_d) with shape function cut by crack interior (excluding the nodes in Ω_c).

In Abaqus, an asymptotic crack-tip singularity function is considered only for stationary cracks. For propagating cracks as in this work, crack-tip asymptotic singularity is not considered [29]. To avoid the need to model a stress singularity, the crack propagates across an entire element at a time. The XFEM-based cohesive segment method is used to simulate crack initiation and propagation along an arbitrary, solution-dependent path. Phantom nodes, which are superposed on the real nodes, are used to represent the discontinuity of the cracked elements. Each phantom node is completely constrained to its corresponding real node while the element is intact. When the element is cut through by a crack, the cracked element splits into two parts. Each new element has a combination of real and phantom nodes depending on the orientation of the crack. Each phantom node and its corresponding real node are no longer tied together and can move apart.
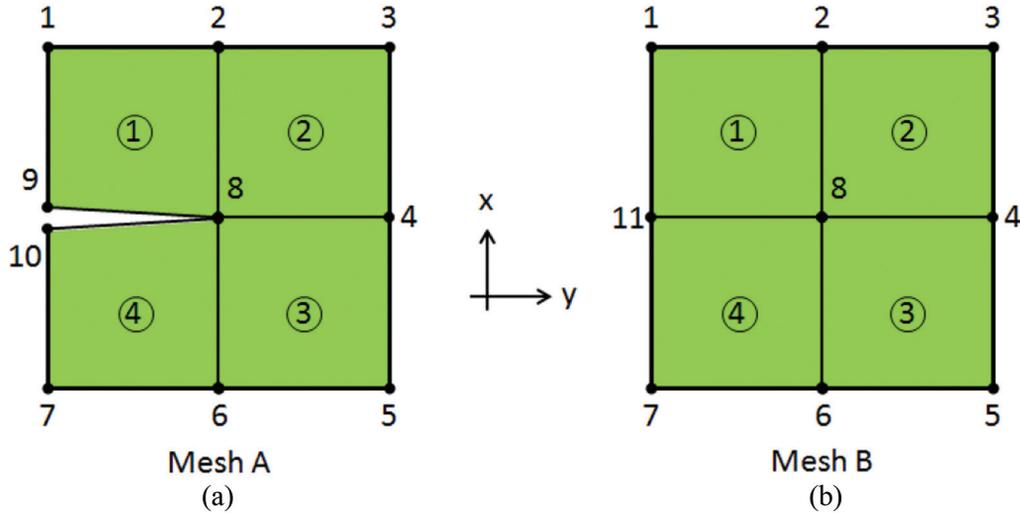
Figure 4. *Finite element mesh: (a) with a crack, (b) without a crack (enrichment).*

3.2. Multi-scale Modeling Approach

The multi-scale configuration used for analyzing the micromechanical fracture behavior is shown in Figure 6. This framework integrates the homogeneous material and mechanical loading at the global level with the fracture mechanism in a heterogeneous material at the local level. The global model includes controlled loading and specimen geometric configuration. The local model constitutes explicit representation of phases in a microstructure. While the global model utilizes elastic properties only, elastic properties and damage parameters (cohesive strength and fracture energy) were used for modeling the microstructure constituents. The model was developed in a commercial finite element code—Abaqus v.6.12 [29].

The global model and the local model were discretized using a 4-node bilinear quadrilateral element (CPE4). A transverse tensile load (displacement) was applied on the global model. The boundary conditions used in the model are illustrated in Figure 6. The local model was modeled as a sub-model (sub-modeling approach in Abaqus) i.e. loads applied on the global model are transferred (interpolated) to the local model through the 'driven nodes' (on the local model). This methodology also ensures that boundary conditions for a RVE are automatically satisfied through the multi-scale modeling approach.

Using the XFEM method, crack initiation and propagation are studied in the local model. Typically, fiber failure under a transverse tensile load is not observed due to weak interfaces. Accordingly, the crack propagation was modeled only in matrix and interface and the XFEM enrichment was active in the matrix only. The fiber/matrix interface was modeled as a cohesive surface. Damage evolution is the critical part of modeling failure in the matrix and the interface.
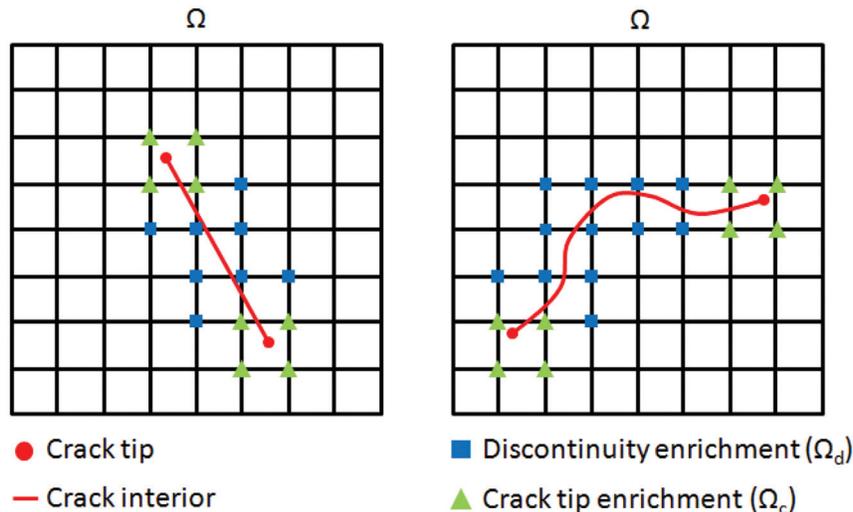

Figure 5. *Nodal enrichment around crack tip and crack interiors.*
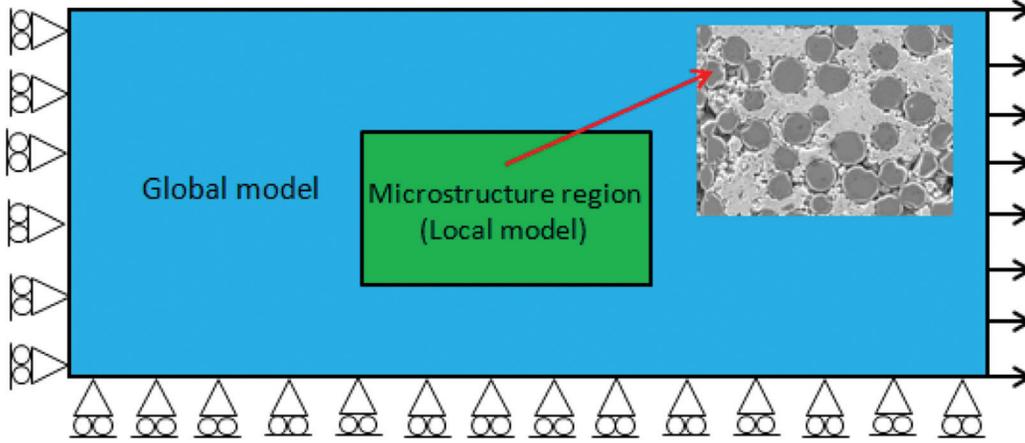
Figure 6. *Multi-scale framework for modeling damage in the microstructure.*

Both the XFEM and cohesive surfaces simulate the failure based on a traction-separation law. A bilinear traction-separation law (Figure 7) was used for modeling the damage initiation and damage evolution. The traction-separation law is characterized by a peak traction 'T_{max}' corresponding to a critical separation 'δ_{max}', and finally by a maximum separation parameter 'δ_{sep}'. In this work, the peak traction parameter corresponds to maximum nominal stress of the material. When the traction stresses are integrated over the separation, the resultant is the energy dissipated 'ϕ' during failure.

$$\phi = \int_0^{\delta_{sep}} T(\delta)d\delta \qquad (13)$$

For the initialization of damage in the cohesive zone, it has to satisfy certain damage initiation criterion. Several damage initiation criteria are available. In this work, the maximum stress criterion based damage initiation has been implemented. Once the damage has initiated, the damage evolution is described by introducing a stiffness degradation parameter, D. The value of D ranges from 0 (no damage) to 1 (complete damage) and can be described by either linear or exponential evolution. For linear softening, the evolution of damage variable 'D' is given by,

$$D = \frac{\delta^f (\delta^{max} - \delta^o)}{\delta^{max}(\delta^f - \delta^o)} \qquad (14)$$

In Equation (14), δ^f is the effective separation at complete failure, δ^o is the effective separation at damage initiation, and δ^{max} is the maximum value of effective separation attained during the loading history. The effective separation at complete failure can be approximated by,

$$\delta^f = \frac{2G}{T_{eff}} \qquad (15)$$

Here, G is the energy dissipated during failure, and T_{eff} corresponds to the peak stress at damage initiation.

4. RESULTS AND DISCUSSION

4.1. Model Validation Using a Benchmark Study

The benchmark study by Fang *et al.* [10] is a representative volume element (RVE) of a ceramic matrix composite under transverse tensile loading. The authors in this benchmark study have developed an approach to estimate the ply level strength and toughness as a function of its microstructural attributes (fiber, matrix, and interface). The authors have developed an augmented finite element method (AFEM) for simulating arbitrary cracking in the ceramic matrix, and proposed augmented cohesive zone elements for modeling the fiber/matrix interface. The RVE developed by the authors had circular fibers of 10 μm diameter and fiber volume fraction was 50%. In the current study, the finite element mesh shown in Figure 3 is used as the RVE. This
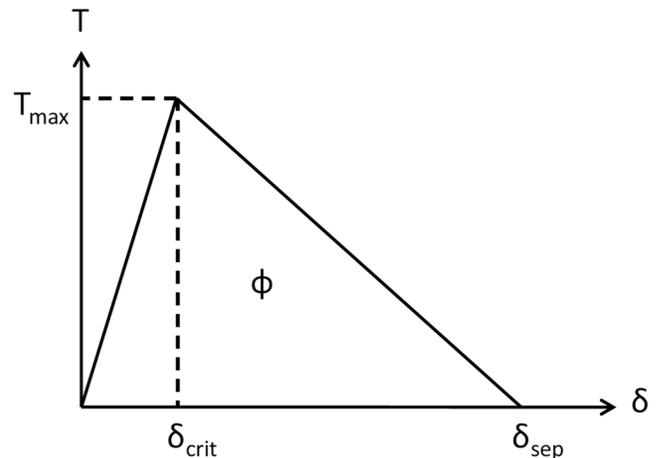

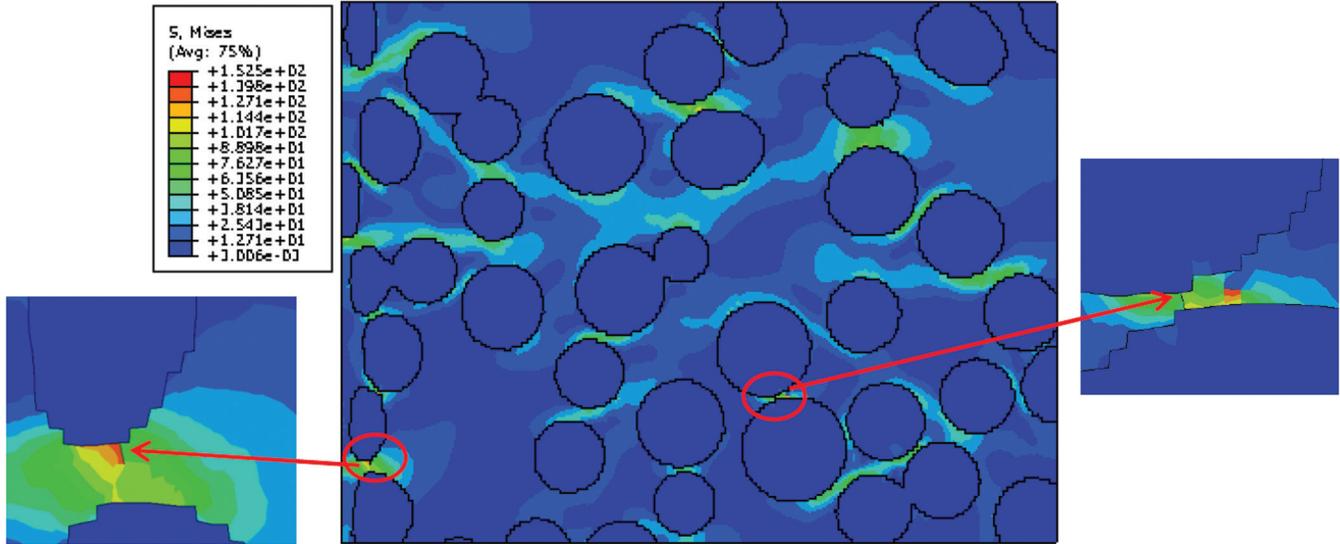**Figure 7.** *Traction-separation law for modeling damage evolution.*

Figure 8. *Matrix crack initiation.*

microstructure had a fiber volume fraction of 44.71%. The material properties of the constituent phases of a ceramic matrix composite have been obtained from the benchmark study [10]. Both fiber and matrix are assumed to be isotropic. The elastic modulus and Poisson's ratio of the fiber are $E_f = 40$ GPa and $v_f = 0.3$. Similarly, the matrix properties are $E_m = 200$ GPa and $v_m = 0.35$. The fracture parameters for this case are: matrix cohesive strength ($T_{max,m}$) = 150 MPa, matrix fracture energy (ϕ_m) = 20 J/m^2, interface cohesive strength ($T_{max,i}$) = 10 MPa, and interface fracture energy (ϕ_i) = 10 J/m^2. Fracture in fibers was not considered.

Due to the applied transverse tensile load, multiple crack initiation sites were observed in the matrix. Figure 8 shows the formation of matrix cracks in the local model. The discontinuities in these locations indicates crack initiation phase i.e. damage initiation criterion was satisfied in the traction-separation law. The evolution of these cohesive cracks into

a complete crack depends on building up of local stresses. Multiple cracks that were initiated in the microstructure have propagated to a fiber/matrix interface. This resulted in failure of the interfaces in these regions. With an increase in applied stress, more cracks were initiated and propagated, leading to an establishment of a complete crack (Figure 9).

The stress-displacement behavior was modeled for the benchmark test case and compared with the results provided by Fang *et al.* [10]. The stress vs. displacement behavior of the RVE was estimated from elastic and fracture parameters of constituent phases, as shown in Figure 10. The peak stress and displacement were predicted to be lower as compared to the benchmark study. The peak stress predicted using the current model was 30.19 MPa while the benchmark result was 35.83 MPa. The variation of predicted peak stress from this value was 15.74%. This difference was assumed to be due to multiple factors—a range of fiber sizes in the microstructure, fiber packing, and fiber volume fraction.
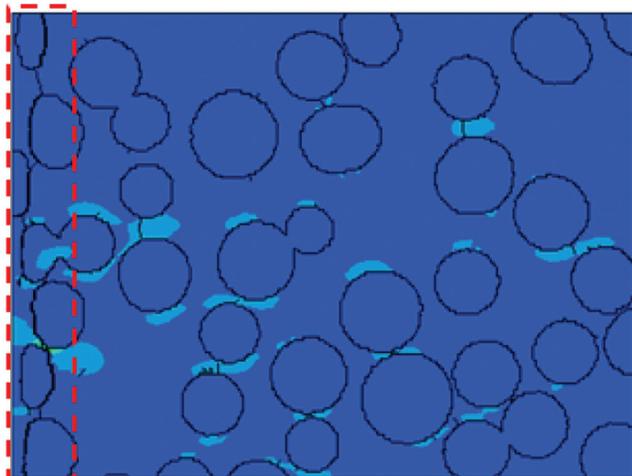

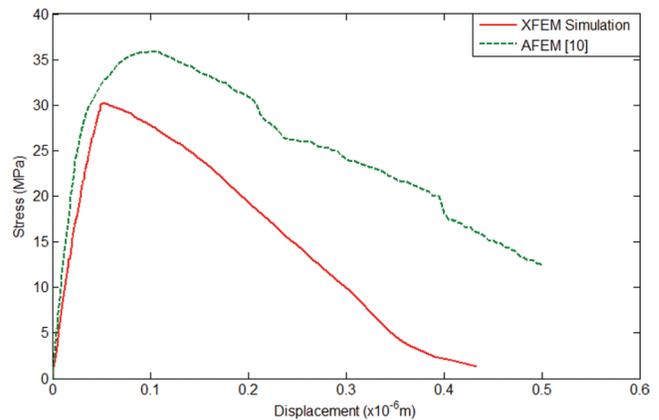**Figure 9.** *Development of a complete crack in the microstructure.*

Figure 10. *Comparison of predicted stress vs. displacement behavior with benchmark results.*

**Table 1.** *Material Properties of Constituent Phases in a SiC/SiC_f Ceramic Composite [30].*

| Material	Modulus E (GPa)	Poisson's Ratio v	Cohesive Strength T_{max} (MPa)	Fracture Energy ϕ (J/m^2)
SiC matrix	350	0.21	300	2
SiC fiber	270	0.2	2800	20
Interface	–	–	10	2

4.2. Failure Analysis of a CFCC Microstructure

The validated model was extended to a unidirectionally reinforced CFCC microstructure. The elastic and fracture properties of a SiC/SiC$_f$ ceramic composite were used as an example to model the microstructure. Table 1 shows the material properties of the constituent phases, required for the numerical simulation. Similar to the benchmark study, the failure of matrix and interface is governed by a traction-separation law. The XFEM enrichment was applied to the matrix region and interface was modeled as a cohesive surface.

The influence of cohesive parameters of the matrix on the predicted stress-displacement behavior (traction-separation) of the RVE was evaluated. The effect of matrix strength was evaluated at three strength levels—200 MPa, 250 MPa, and 300 MPa (Figure 11). It was observed that the strength of the RVE increased with the increase in matrix strength. The strength of the RVE increased by 14.74% and 20.84% by increasing the matrix strength from 200 MPa to 250 MPa and 300 MPa, respectively. In the predicted stress-displacement behavior using the developed model, drop in the load bearing capacity was observed prior to the final failure. This behavior was due to the damage evolution process which is governed by the cohesive damage model. When a crack propagated in the matrix, or when it propagated through the interfaces, these instantaneous jumps were observed.

Figure 12 shows the influence of matrix toughness on the observed stress-displacement behavior. The matrix tough-
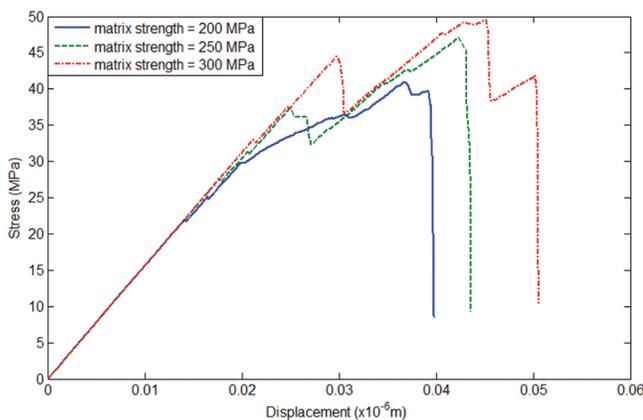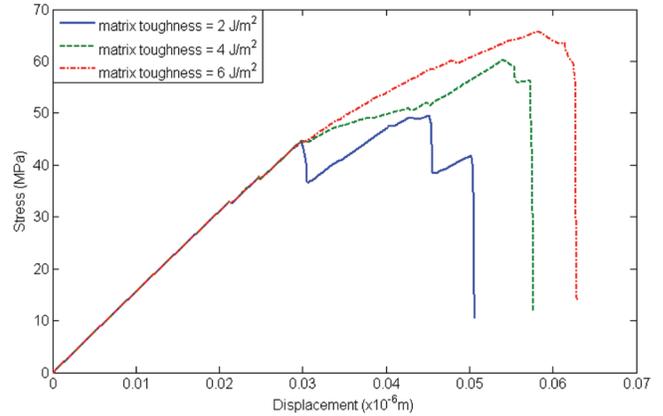
Figure 12. *Effect of matrix toughness on stress-displacement behavior in the microstructure.*

ness was evaluated at three levels—2 J/m^2, 4 J/m^2 and 6 J/m^2. Due to the increase in the matrix toughness, the damage evolution behavior was observed to be stabilized. By increasing the matrix toughness from 2 J/m^2 to 4 J/m^2 and 6 J/m^2, the predicted strengths of the RVE increased by 17.74% and 24.73%, respectively. Also, the increase in the matrix toughness resulted in an increase in the critical displacement on stress-displacement curve.

5. CONCLUSIONS

In this study, a modeling framework was developed for studying the failure behavior in a CFCC microstructure. A finite element mesh was generated on an actual microstructure image of a unidirectionally reinforced CFCC. An XFEM method was integrated into the modeling framework to simulate crack propagation in the microstructure. The developed model was validated by comparing with a benchmark study from technical literature. The effect of cohesive damage modeling parameters of the matrix on the predicted stress-displacement behavior of the RVE was evaluated. By increasing the matrix strength from 200 MPa to 250 MPa and 300 MPa, there was a 14.74% and 20.84% increase in the predicted strength. Also, by increasing the matrix toughness from 2 J/m^2 to 4 J/m^2 and 6 J/m^2, the predicted strengths increased by 17.74% and 24.73%, respectively. The predicted stress-displacement behavior showed an instantaneous drop in the load bearing capacity prior to the final failure. This behavior was observed when the crack propagated in the matrix or through the fiber/matrix interface. The damage evolution, as described by the traction-separation law, was found to be critical to the predicted stress-displacement behavior.

6. ACKNOWLEDGEMENTS

Figure 11. *Effect of matrix strength on stress-displacement behavior in the microstructure.*

7. REFERENCES

[1] N. Chawla, B. V. Patel, M. Koopman, K. K. Chawla, R. Saha, B. R. Patterson, E. R. Fuller, and S. A. Langer, "Microstructure-Based Simulation of Thermomechanical Behavior of Composite Materials by Object-Oriented Finite Element Analysis," *Materials Characterization*, Vol. 49, pp. 395–407, 2002. http://dx.doi.org/10.1016/S1044-5803(03)00054-8

[2] S. Langer, E. R. Fuller, and W. C. Carter, "OOF: An Image-Based Finite-Element Analysis of Material Microstructures," *Computing in Science and Engineering*, Vol. 3, pp. 15–23, 2001. http://dx.doi.org/10.1109/5992.919261

[3] A. C. E. Reid, S. A. Langer, R. C. Lua, V. R. Coffman, S. –I. Haan, and R. E. Garcia, "Image-Based Finite Element Mesh Construction for Material Microstructures," *Computational Material Science*, Vol. 43, pp. 989–999, 2008. http://dx.doi.org/10.1016/j.commatsci.2008.02.016

[4] A. C. E. Reid, R. C. Lua, R. E. Garcia, V. R. Coffman, and S. A. Langer, "Modeling Microstructures with OOF2," *International Journal of Materials and Product Technology*, Vol. 35, pp. 361–373, 2009.http://dx.doi.org/10.1504/IJMPT.2009.025687

[5] V. R. Coffman, A. C. E. Reid, S. A. Langer, and G. Dogan, "OOF3D: An Image-Based Finite Element Solver for Materials Science," *Mathematics and Computers in Simulation*, Vol. 82, pp. 2951–2961, 2012. http://dx.doi.org/10.1016/j.matcom.2012.03.003

[6] A. C. Lewis and A. B. Geltmacher, "Image-Based Modeling of the Response of Experimental 3D Microstructures to Mechanical Loading," *Scripta Materialia*, Vol. 55, pp. 81–85, 2006. http://dx.doi.org/10.1016/j.scriptamat.2006.01.043

[7] A. Goel, K. K. Chawla, U. K. Vaidya, N. Chawla, and M. Koopman, "Two-Dimensional Microstructure Based Modeling of Young's Modulus of Long Fibre Thermoplastic Composite," *Materials Science and Technology*, Vol. 24, pp. 864–869, 2008. http://dx.doi.org/10.1179/174328408X294080

[8] Y. Dong and D. Bhattacharyya, "Morphological-Image Analysis Based Numerical Modeling of Organoclay Filled Nanocomposites," *Mechanics of Advanced Materials and Structures*, Vol. 17, pp. 534–541, 2010. http://dx.doi.org/10.1080/15376490903399746

[9] S. R. Bakshi, A. Bhargava, S. Mohammadizadeh, A. Agarwal, and I. Tsukanov, "Computational Estimation of Elastic Properties of Spark Plasma Sintered TaC by Meshfree and Finite Element Methods," *Computational Material Science*, Vol. 50, pp. 2615–2620, 2011. http://dx.doi.org/10.1016/j.commatsci.2011.04.003

[10] X. Fang, Q. Yang, B. Cox, and Z. Zhou, "An Augmented Cohesive Zone Element for Arbitrary Crack Coalescence and Bifurcation in Heterogeneous Materials," *International Journal of Numerical Methods in Engineering*, Vol. 88, pp. 841–861, 2011. http://dx.doi.org/10.1002/nme.3200

[11] T. Hettich, A. Hund, and E. Ramm, "Modeling of Failure in Composites by X-FEM and Level Sets within a Multiscale Framework," *Computer Methods in Applied Mechanics and Engineering*, Vol. 197, pp. 414–424, 2008. http://dx.doi.org/10.1016/j.cma.2007.07.017

[12] B. Cox and Q. Yang, "In Quest of Virtual Tests for Structural Composites," *Science*, Vol. 314, pp. 1102–1107, 2006. http://dx.doi.org/10.1126/science.1131624

[13] Y. Li and M. Zhou, "Prediction of Fracture Toughness of Ceramic Composites as Function of Microstructure: I. Numerical Simulations," *Journal of the Mechanics and Physics of Solids*, Vol. 61, pp. 472–488, 2013. http://dx.doi.org/10.1016/j.jmps.2012.09.013

[14] C. Gonzalez and J. Llorca, "Multiscale Modeling of Fracture in Fiber-reinforced Composites," *Acta Materialia*, Vol. 54, pp. 4171–4181, 2006. http://dx.doi.org/10.1016/j.actamat.2006.05.007

[15] D. Huynh and T. Belytschko, "The Extended Finite Element Method for Fracture in Composite Materials," *International Journal for Numerical Methods in Engineering*, Vol. 77, pp. 214–239, 2009. http://dx.doi.org/10.1002/nme.2411

[16] R. de Borst, "Numerical Aspects of Cohesive Zone Models," *Engineering Fracture Mechanics*, Vol. 70, pp. 1743–1757, 2003. http://dx.doi.org/10.1016/S0013-7944(03)00122-X

[17] J. Melenk and I. Bubaska, "The Partition of Unity Finite Element Method: Basic Theory and Applications," *Computational methods in Applied Mechanics and Engineering*, Vol. 139, pp. 289–314, 1996. http://dx.doi.org/10.1016/S0045-7825(96)01087-0

[18] N. Moës, J. Dolbow, and T. Belytschko, "A Finite Element Method for Crack Growth Without Remeshing," *International Journal for Numerical Methods in Engineering*, Vol. 46, pp. 132–150, 1999. http://dx.doi.org/10.1002/(SICI)1097-0207(19990910)46:1<131::AID-NME726>3.0.CO;2-J

[19] S. Loehnert and T. Belytschko, "A Multiscale Projection Method for Macro/Microcrack Simulations," *International Journal for Numerical Methods in Engineering*, Vol. 71, pp. 1466–1482. http://dx.doi.org/10.1002/nme.2001

[20] T. Belytschko and T. Black, "Elastic Crack Growth in Finite Elements with Minimal Remeshing," *International Journal for Numerical Methods in Engineering*, Vol. 45, pp. 601–620, 1999. http://dx.doi.org/10.1002/(SICI)1097-0207(19990620)45:5<601::AID-NME598>3.0.CO;2-S

[21] J. Jung and E. Taciroglu, "Modeling and Identification of an Arbitrary Shaped Scatterer Using Dynamic XFEM with Cubic Splines," *Computer Methods in Applied Mechanics and Engineering*, Vol. 278, pp. 101–118, 2014. http://dx.doi.org/10.1016/j.cma.2014.05.001

[22] D. Ling, Q. Yang, and B. Cox, "An Augmented Finite Element Method for Modeling Arbitrary Discontinuities in Composite Materials," *International Journal of Fracture*, Vol. 156, pp. 53–73, 2009. http://dx.doi.org/10.1007/s10704-009-9347-2

[23] Y. Sun, Y. Hu, and K. Liew, "A Mesh-free Simulation of Cracking and Failure using Cohesive Segments Method," *International Journal of Engineering Science*, Vol. 45, pp. 541–553, 2007. http://dx.doi.org/10.1016/j.ijengsci.2007.03.004

[24] E. Barbieri and M. Meo, "A Meshfree Penalty-based Approach to Delamination in Composites," *Composites Science and Technology*, Vol. 69, pp. 2169–2177, 2009. http://dx.doi.org/10.1016/j.compscitech.2009.05.015

[25] T. Rabczuk, "Computational Methods for Fracture in Brittle and Quasi-Brittle Solids: State-of-the-Art Review and Fracture Perspectives," *ISRN Applied Mathematics*, Vol. 2013, Article ID 849231, pp. 1–38, 2013.

[26] G. Ventura, J. Xu, and T. Belytschko, "A Vector Level Set Method and New Discontinuity Approximations for Crack Growth by EFG," *International Journal for Numerical Methods in Engineering*, Vol. 54, pp. 923–944, 2002. http://dx.doi.org/10.1002/nme.471

[27] M. Fleming, Y. Chu, B. Moran, and T. Belytschko, "Enriched Element-free Galerkin Methods for Crack Tip Fields," *International Journal for Numerical Methods in Engineering*, Vol. 40, pp. 1483–1504, 1997. http://dx.doi.org/10.1002/(SICI)1097-0207(19970430)40:8<1483::AID-NME123>3.0.CO;2-6

[28] P. Michlik and C. Berndt, "Image-based Extended Finite Element Modeling of Thermal Barrier Coatings," *Surface & Coatings Technology*, Vol. 201, pp. 2369–2380, 2006. http://dx.doi.org/10.1016/j.surfcoat.2006.04.003

[29] ABAQUS/Standard User's Manual, Vol. I and II (ver. 6.12), 2012. Hibbit, Karlsson and Sorensen, Inc., Pawtucket, Rhode Island.

[30] S. Liu, L. Zhang, X. Yin, L. Cheng, and Y. Liu, "Microstructure and Mechanical Properties of SiC and Carbon Hybrid Fiber Reinforced SiC Matrix Composite," *International Journal of Applied Ceramic Technology*, Vol. 8, pp. 308–316, 2011. http://dx.doi.org/10.1111/j.1744-7402.2010.02588.x